INTERNATIONAL JOURNAL FOR NUMERICAL METHODS IN FLUIDS, VOL. 6, 557–572 (1986)

AN EFFICIENT ALGORITHM FOR SOLVING THE INCOMPRESSIBLE FLUID FLOW EQUATIONS

V. M. THEODOSSIOU AND A. C. M. SOUSA

Department of Mechanical Engineering University of New Brunswick, Fredericton, N. B., Canada E3B 5A3

SUMMARY

The present paper reports on a modified pressure implicit predictor–corrector type scheme for solving the flow governing equations, in which a consistent formulation is combined with a multi-grid solver for the pressure correction. In addition a parabolic sublayer (PSL) approach for the treatment of the flow in the vicinity of solid walls is critically evaluated in terms of accuracy and computational efficiency. The lid-driven cavity flow is chosen as the test case and results are presented for Reynolds numbers ranging from 100 to 1000. Predictions with the proposed scheme indicate substantial computational savings and fairly good agreement when compared with previous work. The PSL approach reduces the computing time, but with increasing Reynolds numbers the accuracy of the solutions tends to deteriorate.

KEY WORDS Navier–Stokes Equations Primitive Variables Parabolic Sublayer Approach Multi-grid Method

INTRODUCTION

The numerical study of turbulent or high Reynolds number laminar flows requires a special treatment in the near-wall region. Typically, mesh refinement is used, but this approach tends to slow down convergence rates quite dramatically. For this reason, as an alternative in turbulent flows, wall functions are employed. These functions, however, are in most cases simple formulae based on experimental data for parallel flows with dubious applicability to recirculating flows. Two recent papers[1,2] examine this particular problem and they propose that the near-wall region flow be treated as a parabolic syblayer (PSL) with constant pressure across it. This approach is of some merit; however, concern has been expressed on the suitability of the PSL for regions in the vicinity of a stagnation point, where large variations of pressure normal to the wall may occur.

This work investigates the validity of the PSL approach for the lid-driven cavity flow, since strong recirculating eddies are present in such a configuration. Concurrently an efficient numerical scheme based on the SIMPLEC algorithm[3] incorporating a fast multi-grid numerical solver,[4] is discussed and analysed. Results with and without the PSL approach are compared to each other and with work of previous authors for different Reynolds numbers.

MODEL PROBLEM

The fluid motion generated in a square cavity by the uniform translation of the upper surface of the cavity is a classic example of recirculating flow. Cavity flows have attracted considerable attention in recent years,[5,6] owing to their many practical implications. From a purely computational viewpoint, the cavity flow is an ideal prototype non-linear problem which is

0271–2091/86/080557–16$08.00

Received 14 June 1985
Revised 13 February 1986

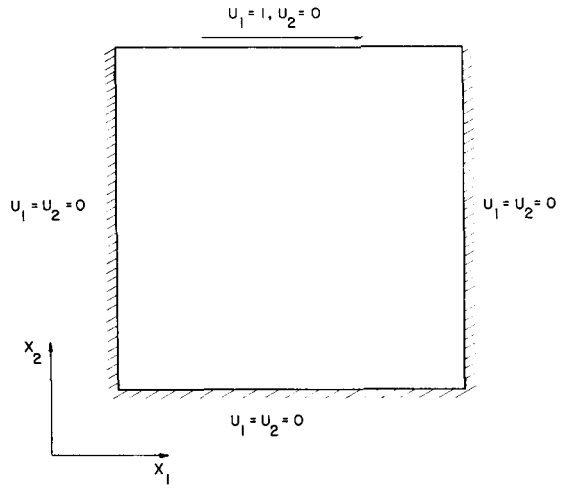

Figure 1. Cavity problem, definition

readily posed for numerical solution. Its geometric simplicity (Figure 1), and comparatively minor singularities make it very attractive as a test case for new numerical techniques, and as a benchmark solution to evaluate competing schemes using different approaches for problem formulation, discretization and computational procedure.

The two-dimensional, steady, laminar motion of an incompressible Newtonian fluid is considered. Steady-state conditions are assumed for the flow, but the numerical solution is obtained through a quasi-transient procedure starting from rest.

The non-dimensional flow governing equations in Cartesian-tensorial notation are:

Conservation of momentum

$$\frac{\partial u_i}{\partial t}+\frac{\partial (u_i u_j)}{\partial x_j}=\frac{\partial}{\partial x_j}\left(\frac{1}{Re}\frac{\partial u_i}{\partial x_j}\right)-\frac{\partial P}{\partial x_i}, \qquad i=1,2;\ j=1,2. \tag{1}$$

Conservation of mass

$$\frac{\partial u_i}{\partial x_i}=0, \qquad i=1,2. \tag{2}$$

The Reynolds number (Re) in equation (1) is based on the velocity of the upper moving boundary.

NUMERICAL METHOD

Discretization procedure

The conservation equations are discretized by an averaging procedure over small control domains surrounding nodal points. A staggered grid structure[7] is adopted, in which the pressure is defined in the centre of the control volume, and velocity components are located at the centres of the control volume faces (Figure 2). This arrangement has the convenient feature that the velocity components are stored at just the points at which they are required for the calculation of their

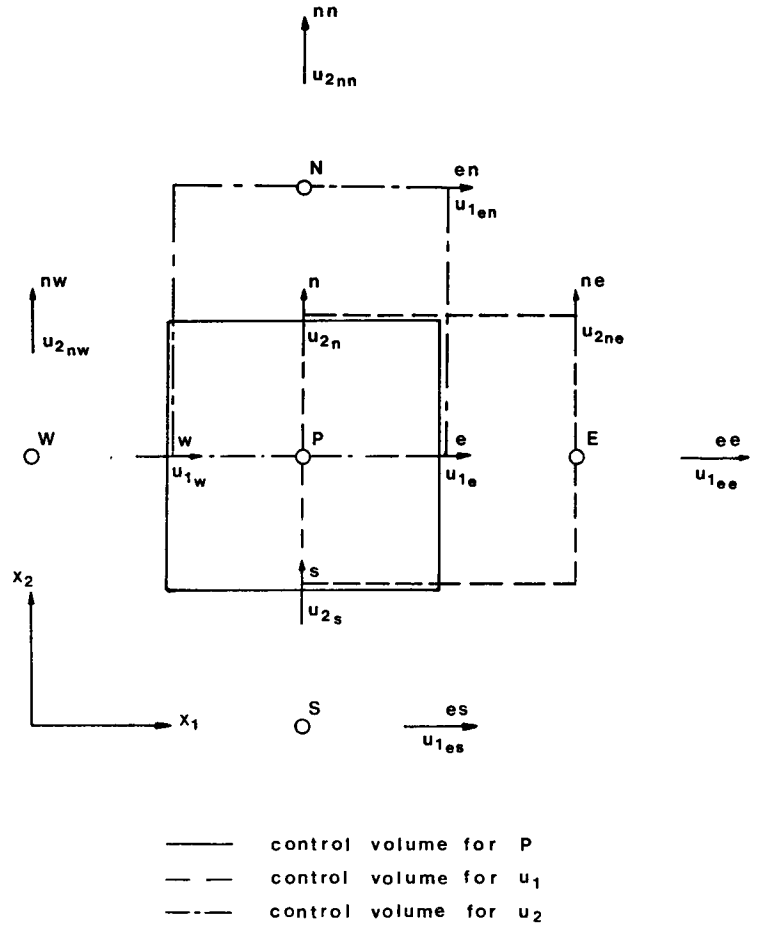

Figure 2. Staggered control volume arrangements

advective contribution, and the pressure gradients in the momentum equations can be represented by central differences without inducing non-physical oscillations in the pressure distribution.

The convection–diffusion flux terms are approximated by a hybrid upwind/central discretization scheme.[8] This formulation, based on numerical experiments reported elsewhere,[9] proved to be a reasonable compromise between accuracy and computational effort.

Underrelaxation, E-factor formulation

Following the generalized formulation of Patankar,[10] the discretized equations are written for the general variable Φ as

$$a_P\Phi_P = a_E\Phi_E + a_W\Phi_W + a_N\Phi_N + a_S\Phi_S + b. \tag{3}$$

This equation is formally presented as linear, but in fact the coefficients are functions of Φ. To account for the inter-equation linkages and non-linearities, repeated cycles ('solutions') of the set of discretization equations similar to equation (3) are performed with the coefficients 'frozen' for each cycle. The cycle-by-cycle change of the coefficients may result in large changes of the Φ-values, leading eventually to slow convergence or even divergence. To moderate the changes in

consecutive 'solutions' for Φ, and thereby to improve convergence, underrelaxation can be introduced into equation (3) as follows:

$$\frac{a_P}{\alpha}\Phi_P = \sum a_{nb}\Phi_{nb} + b + \frac{1-\alpha}{\alpha}a_P\Phi_P^0, \tag{4}$$

where Φ_P^0 is the value of Φ_P from the previous cycle, and α is the underrelaxation factor.

Raithby and Schneider[11] introduced the E-factor into the discretized equation (4), which can be rewritten as

$$a_P\left(1+\frac{1}{E}\right)\Phi_P = \sum a_{nb}\Phi_{nb} + b + \frac{a_P}{E}\Phi_P^0. \tag{5}$$

The primary reason for transforming equation (4) into equation (5) is that E lends itself to direct physical interpretation. Equation (5) is precisely the equation that results when the transient term is retained in equation (1), so that the solution of equation (5) advances Φ through a time step Δt which is proportional to the maximum allowable time step Δt^* for an explicit formulation, i.e.

$$\Delta t = E\Delta t^*, \quad \text{where} \quad \Delta t^* = \frac{\rho \Delta V}{a_P}.$$

With a constant E-factor, the value of Δt^* will change from one control volume to the next, and Φ will be advanced non-uniformly in time across the grid. This skewed transient is desirable as a means of accelerating convergence.[11,12] Values of E in the range of 2 to 10 are commonly used.[3,11,13]

The SIMPLEC algorithm

The SIMPLEC algorithm[3] is a predictor–corrector type scheme, in which the momentum equations are linked to the continuity equation by the pressure correction equation.

To illustrate the numerical procedure, a brief outline of the computational steps is given for the velocity component in the x_1-direction, u_1, as follows:

1. Determination of the velocity u_1^* using a tentative value for pressure (P^*) in the x_1-direction momentum equation:

$$a_e u_{1_e}^* = \sum a_{nb} u_{1_{nb}} + (P_P^* - P_E^*)A_e + b_e, \tag{6}$$

where A_e is the area of the domain on which the pressure difference is applied, and

$$a_e\left(\sum a_{nb} - S_e\Delta V\right)\left(1+\frac{1}{E}\right). \tag{7}$$

2. Solution of the pressure correction (P') equation:

$$a_P P_P' = \sum a_{nb} P_{nb}' + b_P, \tag{8}$$

where b_P represents a mass imbalance term, given by

$$b_P = (\rho u_1^* A)_w - (\rho u_1^* A)_e + (\rho u_2^* A)_s - (\rho u_2^* A)_n. \tag{9}$$

3. Correction of the velocity field to satisfy continuity:

$$u_{1_e} = u_{1_e}^* d_e(P_P' - P_E'), \tag{10}$$

where

$$d_e = \frac{A_e}{a_e - \sum a_{nb}}. \tag{11}$$

4. Updating of the pressure field:

$$P = P^* + P'. \tag{12}$$

At this stage convergence criteria are checked, and if they are satisfied the calculation is stopped; otherwise the computational procedure is repeated from step 1, with P taking the place of P^*.

The measure of convergence of the solution is given by equation (9). When b_P is a vanishingly small value ($|b_P| < 10^{-5}$) for all control domains of the finest mesh, and the velocity field remains practically the same from cycle to cycle, the iterative process is stopped.

Boundary conditions

In order to solve the system of the discretized momentum equations and the pressure correction equation, appropriate boundary conditions must be imposed. The boundaries of the flow domain are taken as non-slip and impermeable; consequently the velocity components at the walls are zero, except for the dimensionless tangential component of the velocity at the moving wall, which takes the value of 1 (Figure 1). Owing to the staggered grid arrangement employed, not all the variables have grid points on all the boundaries; for example, there is no vertical velocity node on a vertical wall, nor a horizontal velocity node on a horizontal wall. In such cases the boundary conditions are imposed by extrapolating the boundary value of the variable to a fictitious point that lies outside the solution domain.

Since the normal velocity components are prescribed at all boundaries, the flow rates across the boundary faces are not expressed in terms of u_1^* and u_2^*, but in terms of the actual velocities u_1 and u_2. Then, no velocity or pressure corrections are required for these faces; therefore, their corresponding coefficients are set to zero in the pressure correction equation. This is identical to prescribing a zero gradient of P′ on each of the boundaries.

Solution of equations

Owing to the non-linear nature of the problem, the discretized equations are solved by the use of iterative methods.

The solution of the momentum equations represents only a small share of the total cost of solving a fluid flow problem. Since the associated coefficients are only tentative and they change from cycle to cycle, it is wasteful to drive the momentum equations to tight convergence. For the cases examined, adequate convergence is obtained using 5–10 applications of a line-by-line relaxation technique sweeping in the direction of the top moving wall.

The solution of the pressure correction equation (8), can represent as much as 80 per cent of the total computational cost of solving the fluid flow problem.[3] This equation poses a considerable challenge to most of conventional iterative schemes, owing to its strong ellipticity associated with the high anisotropy of the coefficients and the Neumann boundary conditions. These difficulties may be overcome with the use of a multi-grid technique.[4] The multi-grid approach implies the dynamic interaction of the numerical solution over grids of different sizes (levels). The motivation behind this is that common iterative techniques eliminate the high frequency components of the error within the first few iterations, leaving the low frequency error

components almost unchanged, resulting in a slow convergence rate. By employing several grids of different size, the low frequency error components are rapidly annihilated on coarser grids where the computational cost is relatively low. This eventually leads to an acceleration of the overall convergence rate.

There are many types of multi-grid cycles and algorithms which can be applied to a broad range of linear and non-linear problems.[4,14] In this particular study, a cycling–accommodative–correction multi-grid method is employed, which is suitable for linear or artificially linearized (frozen coefficients) problems. The fine–coarse grid arrangement is such that the coarse grid points do not coincide with the fine grid points. An example of such an arrangement employing only two grid levels is shown in Figure 3.

The multi-grid technique may be outlined by considering a series of grids, $G_0, G_1, \ldots, G_k, \ldots, G_m$, with corresponding mesh sizes $h_0 > h_1 > \cdots h_k \cdots > h_m$, all approximating the same domain D. The pressure correction equation (8) for each mesh level k may be represented by

$$L_k P'_k(x_1, x_2) = B_k(x_1, x_2), \quad (x_1, x_2) \in D \tag{13}$$

and associated boundary conditions. The term L_k represents a discrete difference operator, containing the coefficients of the pressure correction equation $(a_P, a_W, a_N, a_E, a_S)$. It should be noted that these coefficients are not constant, but change from point to point within the solution domain, and from cycle to cycle within the computational procedure. Let P''_k be the evolving solution to equation (13). Then the multi-grid method uses the fact that the solution on the next coarser grid G_{k-1} can be improved if the error $E_k = P'_k - P''_k$ and the residual $R_k = B_k - L_k P''_k$ are smooth (low frequencies are dominant), which may be achieved in a few sweeps of a suitable relaxation technique.

An alternative direction line relaxation technique is employed, since it was found to be very

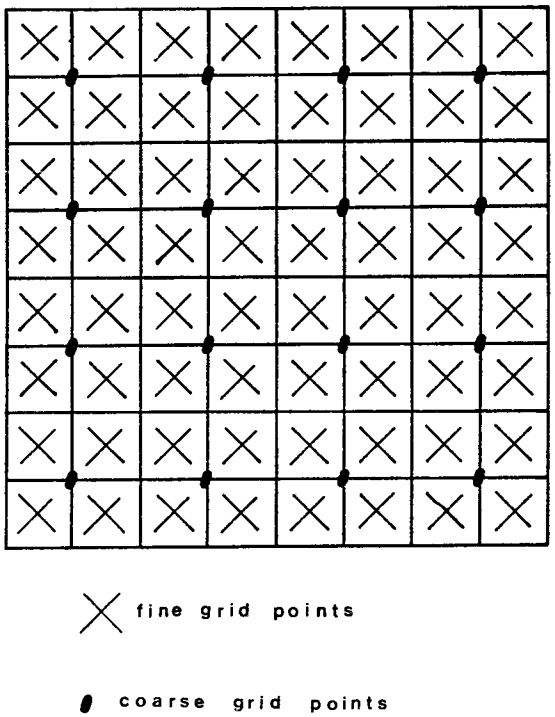

Figure 3. Two cell-centred grids, in which coarse grid unknowns are not a subset of fine grid unknowns

efficient for problems involving anisotropic coefficients.[15] Using the correction multi-grid method, one approximates the residual equation

$$L_k E_k = R_k \quad (\text{on } G_k) \tag{14}$$

by

$$L_{k-1} E_{k-1} = r_k^{k-1} R_k \quad (\text{on } G_{k-1}), \tag{15}$$

where the restriction operator r_k^{k-1} defines the way in which the residuals are transferred from G_k to G_{k-1}. The restriction procedure, as well as the transfer of the coefficients of the pressure correction equation from the fine to the coarse levels are achieved by linear interpolation.

If E_{k-1} is the exact solution of equation (15), P_k'' may be corrected by

$$P_k'' = P_k'' + P_{k-1}^k E_{k-1}, \tag{16}$$

where the prolongation operator P_{k-1}^k stands for a bilinear interpolation procedure to transfer the corrections from G_{k-1} to G_k.

This process is continued iteratively, after smoothing out the high frequencies on P_k'' that are introduced by prolongation. Instead of solving equation (15) exactly, one uses still coarser grids to obtain an approximate solution to the residual equation, and the full procedure is repeated on the coarser grids.

PSL procedure

The parabolic sublayer (PSL) approach is used to resolve the thin boundary layers along the vertical walls of the cavity. Within the sublayer, only the u_2-momentum equation is solved, as the pressure gradient across the layer is assumed to be zero, and the u_1 velocity components are obtained from continuity.

The SIMPLEC procedure is slightly modified in order to account for the PSL treatment of the vertical boundaries. The main steps of the modified algorithm may be summarized as follows:

1. solution of the u_2-momentum equation over the whole computational domain.
2. determination of the u_1 velocity within the PSL, by applying continuity to the pressure domains
3. solution of the u_1-momentum equation over the elliptic region only
4. solution of the pressure correction equation over the elliptic region
5. correction of the velocity field and updating of pressure.

RESULTS AND DISCUSSION

Numerical tests are conducted to evaluate the performance of the multi-grid method and to determine the relative computational efficiency of PSL and its influence upon the solution. In addition the overall accuracy of the numerical algorithm is compared with previously published work.[6]

Multi-grid testing

The excellent convergence performance of the multi-grid method when applied to elliptic equations with uniform coefficients and Dirichlet boundary conditions is well known.[4] By contrast, there is some uncertainty when coefficients are anisotropic and Neumann boundary

conditions are present. Previous work in this area has met only moderate success,[16] or conditions were artificially oversimplified.[9]

For preliminary testing of the version of the multi-grid method developed in the present work, a mesh of 96 × 96 corresponding to the finest level is used. A typical iterative cycle towards the solution of the cavity flow problem with Reynolds number equal to 1000 is used for comparisons among 1-(single-grid), 2- and 3-level methods. The convergence criterion followed is

$$\| r_P^N \| \leqslant \gamma_P \| r_P^0 \| \tag{17}$$

where $\| r_P^N \|$ and $\| r_P^0 \|$ are the Euclidean norms of the residual of the pressure correction equation at iteration level N and at the beginning of the iterative process, respectively, and $\gamma_P = 0{\cdot}05$.

The convergence performance of the multi-grid method as compared to that of a single-grid technique is shown in Figure 4, where one work unit is defined as a full iteration of the alternative direction line relaxation scheme on the finest level. The 3-level multi-grid method requires only 5·125 work units to attain convergence, whereas the single-grid method requires 24 units.

The convergence rate of the multi-grid method, as defined by Brandt,[4] is given by

$$\eta = \left[\frac{\| r_P^N \|}{\| r_P^0 \|} \right]^{1/W}, \tag{18}$$

where W is the number of work units required to attain $\| r_P^N \|$. The convergence rate of the 3-level multi-grid method for the case depicted in Figure 4 is found to be 0·56. This rate of convergence is however, not constant but varies from cycle and from case to case (i.e. Reynolds number and grid size), and for the cases examined it takes values between 0·5 and 0·85.

The overall computational performance of the multi-grid algorithm, as compared to that of a single-grid method, is critically evaluated for a series of test cases using meshes of 24 × 24,

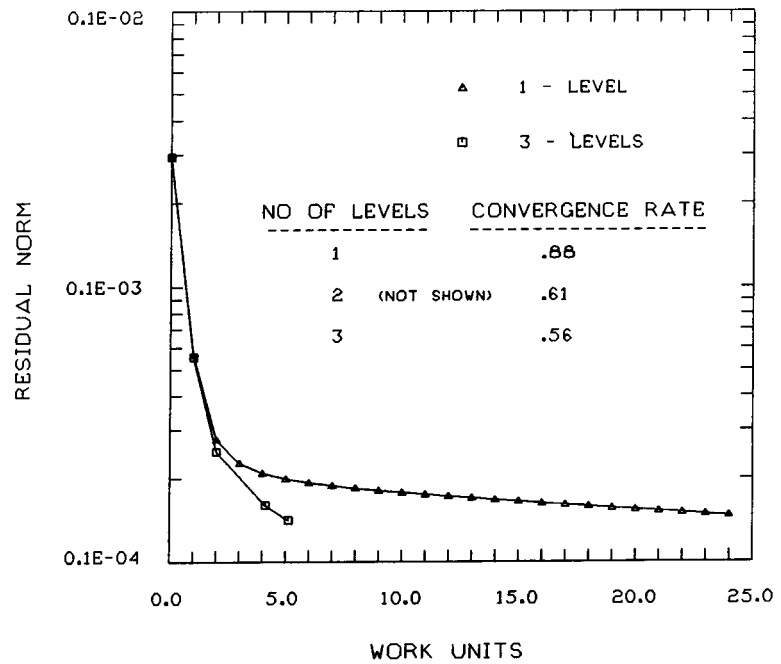

Figure 4. Multi-grid behaviour, for a single cycle of the cavity flow problem. $Re = 1000$, grid = 96 × 96

Table I. Multi-grid computational savings for the solution of the cavity flow problem

	Percentage saving		
		Re	
Grid size	100	1000	10,000
24 × 24	4·2	4·4	5·4
48 × 48	40·5	31·8	30·4
72 × 72	59·4	52·2	50·2
96 × 96	69·1	64·9	62·6

48 × 48, 72 × 72 and 96 × 96, corresponding to the finest level. Solutions to the cavity flow problem are obtained for Reynolds numbers of 100, 1000 and 10,000.

The percentage savings in computational effort obtained by the use of a 3-level multi-grid method over the use of a single-grid method are shown in Table I.

It can be seen that for a 24 × 24 mesh, the multi-grid computational savings are relatively small (4–5 per cent). When finer meshes are employed, the savings are increased, reaching a maximum of 69·1 per cent for a 96 × 96 mesh and a Reynolds number of 100.

Trial runs conducted using 4 and 5 levels did not indicate any appreciable reduction in the computational effort required by the 3-level multi-grid technique.

Algorithm and PSL

The lid-driven cavity flow for a Reynolds number of 100 is solved using an 18 × 18 mesh. The computed velocities are in very good agreement with the results reported in Reference 6 for a vorticity–stream-function formulation and a 129 × 129 grid. The rather coarse mesh, however, cannot resolve the boundary layer flow, particularly along the vertical walls. To overcome this difficulty, each control domain lying along the vertical walls is subdivided into four finer subdomains, resulting in a non-uniform 24 × 18 mesh. The discretization of the flow domain is very successful in predicting the near wall flow (Figure 5), but it requires a considerable

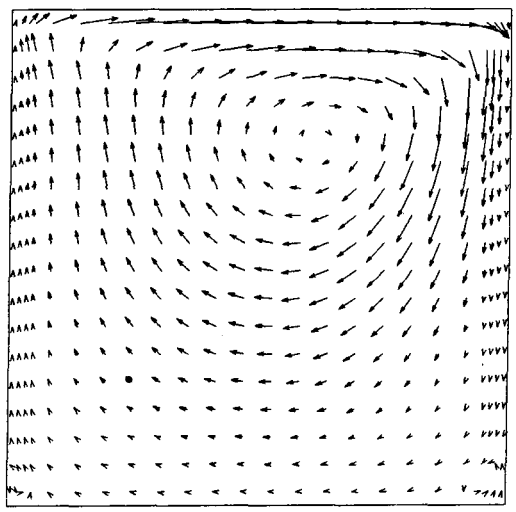

Figure 5. Flow prediction for $Re = 100$ on a 24 × 18 mesh

Table II. Computer time required for the solution of the lid-driven cavity flow for $Re = 100$

Grid	CPU–IBM 3081 (s)
18 × 18	16·31
24 × 18 (fully elliptic)	27·03
24 × 18 (PSL)	17·35

computational effort compared to the 18 × 18 mesh solution, as shown in Table II. Using the same type of discretization the PSL approach yields identical results with the 24 × 18 fully elliptic solution, requiring however 36 per cent less computational effort (Table II).

Figure 6 presents the vertical velocity profile along the centreline in the x_1 direction calculated using a 24 × 18 mesh with and without PSL, and the 129 × 129 mesh solution reported in Reference 6. It can be seen that the three sets of results are almost identical.

The validity of the PSL approach is also examined for higher Reynolds number flows. Figure 7 provides a comparison of the results obtained within the PSL region for $Re = 400$, using a 24 × 18 mesh with and without PSL, and a 64 × 64 fine grid solution. It can be seen that in spite of the fact that the results obtained using the PSL approach do not compare very well with the fine grid predictions, they are almost identical with the 24 × 18 fully elliptic solution. This indicates that the error in the PSL solution is not caused by the assumptions embodied in the PSL treatment of the near-wall flow, but is due to the inherent coarseness of the 24 × 18 mesh.

The results obtained for a $Re = 1000$ case are depicted in Figure 8. They show that the PSL prediction deviates even from the 24 × 18 fully elliptic solution. The reason may be found in the fact that for convection dominated flows (high Reynolds number) the parabolic sublayer, if its existence is assumed, should be confined to very thin regions by the boundary walls. Having in mind that for high Reynolds numbers, relatively fine grids are required to accurately predict the flow, it is expected that the gains of the PSL treatment will be marginal.

Accuracy of the algorithm

The overall accuracy of the numerical scheme and the dependence of the solution on the grid size, are examined by solving the cavity flow problem, using meshes of 18 × 18 to 96 × 96, for Reynolds numbers of 400 and 1000. All computations are performed using an E-factor of 5, since it was found to give the highest convergence rate for the solution procedure.

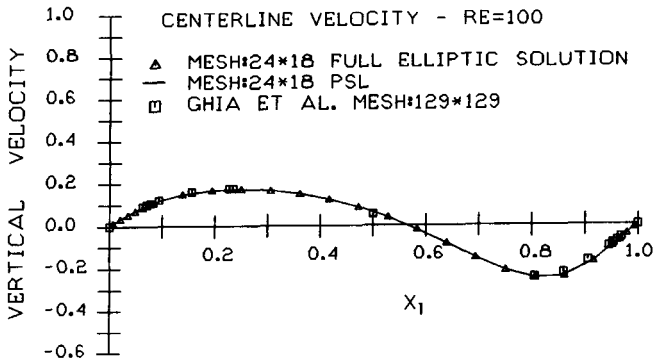

Figure 6. Vertical velocity profile along the x_1-centreline for $Re = 100$

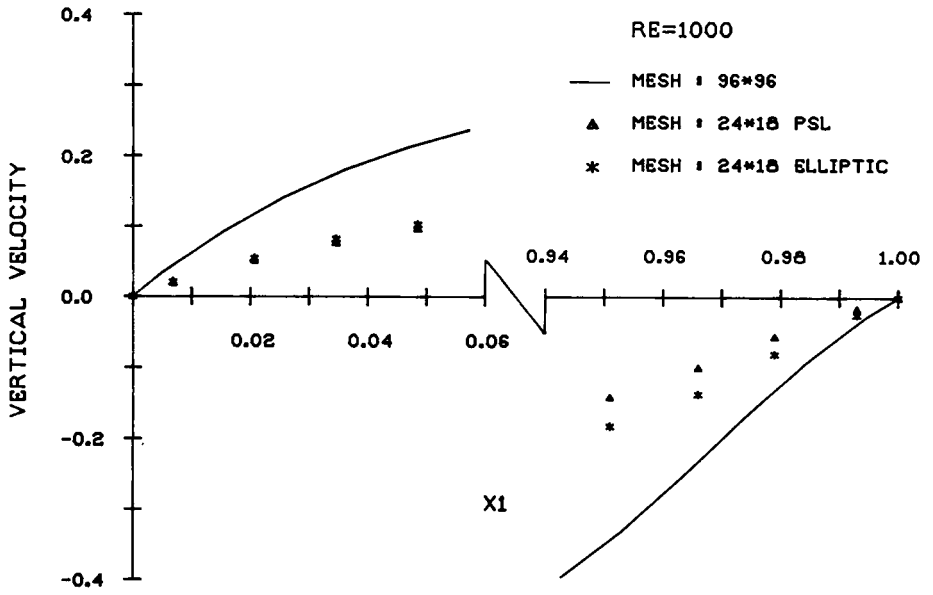

Figure 7. Vertical velocity profile in the PSL region for $Re = 400$

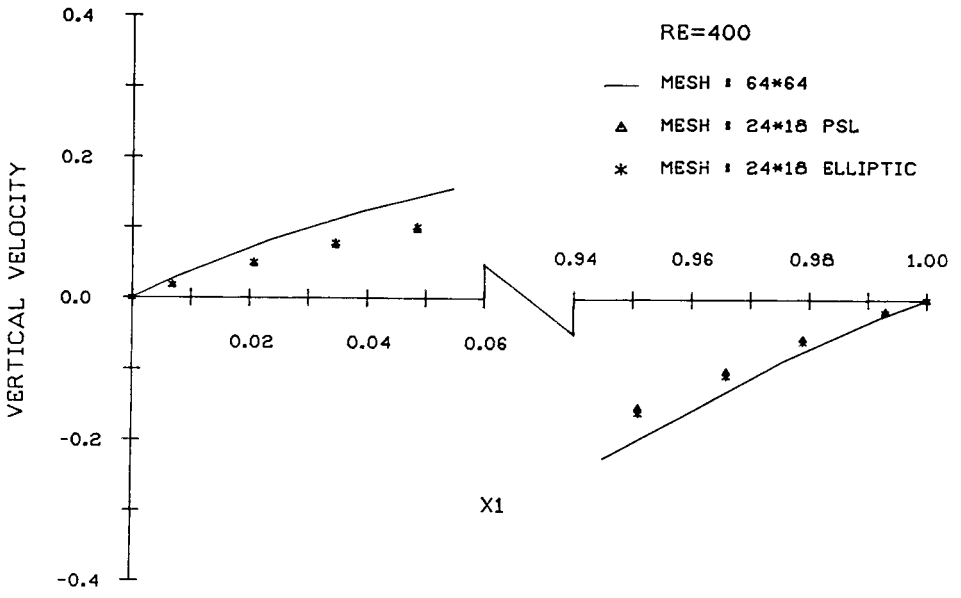

Figure 8. Vertical velocity profile in the PSL region for $Re = 1000$

The numerical simulation of the flows for $Re \geqslant 400$ imposes a considerable computational effort, since the mesh density required to yield accurate solutions is increased with increasing Re. This mesh refinement is required to reduce the effect of artificial diffusion,[10] which increases monotonically with the Reynolds number, and to describe accurately the steep velocity gradients present in the flow. This particular aspect is illustrated in Figure 9, where the horizontal and vertical velocity profiles along the x_2 and x_1 centrelines are plotted for $Re = 400$. It can be seen

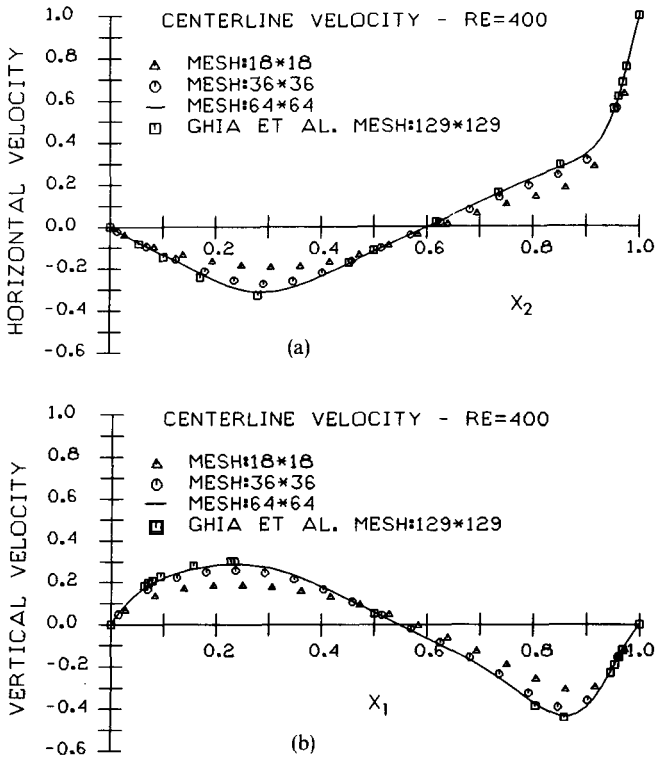

Figure 9. Horizontal (a) and vertical (b) velocity profiles along the x_2 and x_1 centrelines, respectively, for $Re = 400$

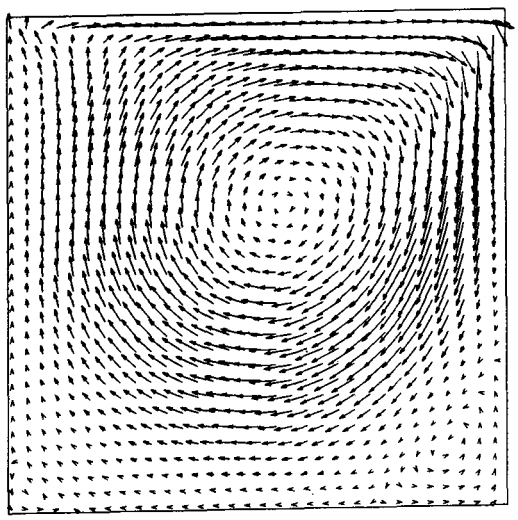

Figure 10. Flow prediction for $Re = 400$ on a 64×64 mesh

that for such a case, even a 36×36 mesh is not adequate to accurately predict the flow. The use of a 64×64 grid, however, yields results that are in very good agreement with the results reported in Reference 6.

The predicted flow field for $Re = 400$ is shown in Figure 10. The primary vortex centre has

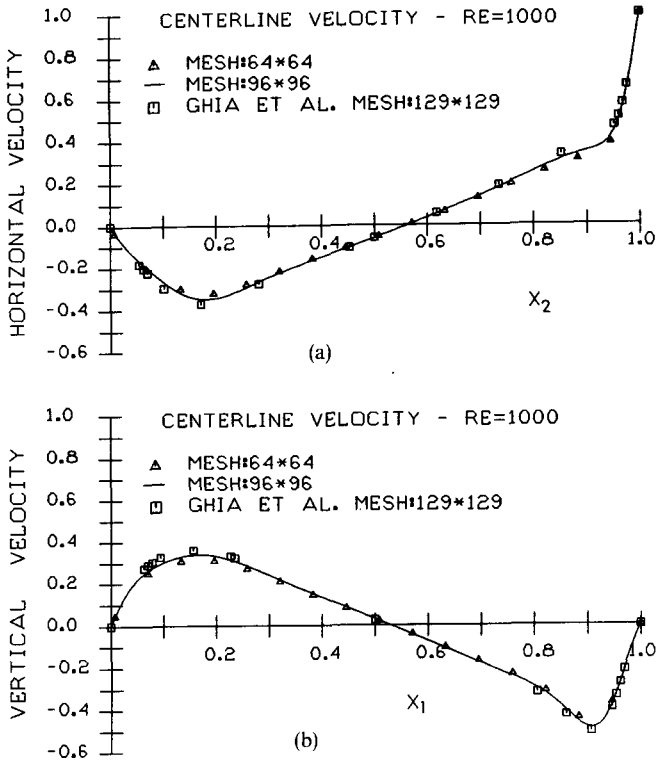

Figure 11. Horizontal (a) and vertical (b) velocity profiles along the x_2 and x_1 centrelines, respectively, for $Re = 1000$

moved towards the geometric centre of the cavity as compared with the $Re = 100$ case (Figure 5), owing to the relative reduction of the viscous stresses resulting from an increase in the Reynolds number.

For the $Re = 1000$ case, a 96×96 mesh produces results of comparable accuracy to those reported by Ghia *et al.*,[6] as shown in Figure 11. As the convective terms become more dominant, the primary vortex centre moves further towards the geometric centre of the cavity (Figure 12). The secondary recirculating eddies at the bottom corners of the cavity become slightly stronger when compared to the $Re = 400$ eddies.

The behaviour of the primary vortex centre as a function of the Reynolds number is illustrated in Figure 13. The vortex centre moves towards the geometric centre of the cavity as the Reynolds number increases and the viscous forces become less dominant. The primary vortex locations predicted by the SIMPLEC-MG scheme are in excellent agreement with the results reported in Reference 6 (Table III).

Table III. Location of primary vortex centre

	$Re = 100$		$Re = 400$		$Re = 1000$	
	SIMPLEC-MG	Reference 6	SIMPLEC-MG	Reference 6	SIMPLEC-MG	Reference 6
x_1	0·614	0·6172	0·555	0·5547	0·531	0·5313
x_2	0·732	0·7344	0·614	0·6055	0·571	0·5625

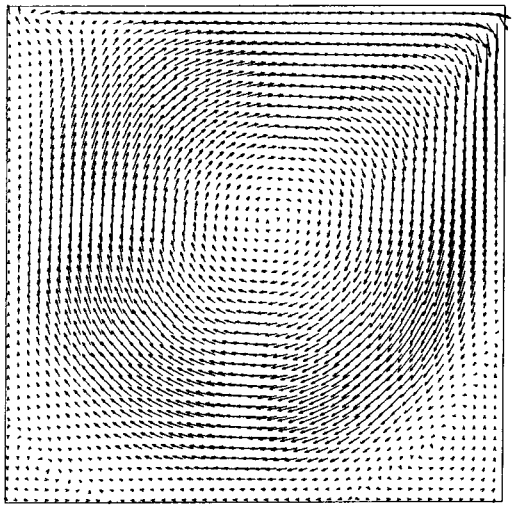

Figure 12. Flow prediction for $Re = 1000$ on a 96×96 grid

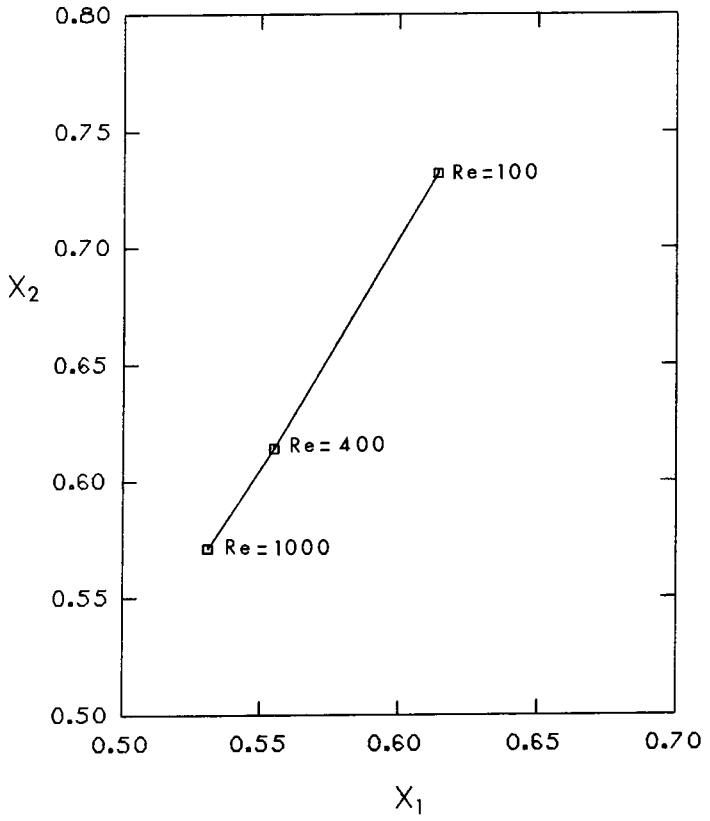

Figure 13. Effect of Reynolds number on location of primary vortex centre

CONCLUDING REMARKS

The proposed scheme, which combines a consistent formulation with a three-level multi-grid solver for the pressure correction equation, leads to substantial computational savings when compared to single-grid methods. The alternate direction line relaxation technique used in the smoothing process of the multi-grid solver was found to be very effective in dealing with the high anisotropy of the coefficients.

The PSL approach shows a reasonable performance, considering its *a priori* limitations for recirculating flows. Its application, however, requires prior estimate of the boundary layer region; the PSL when used in the elliptic region leads to gross inaccuracies.

ACKNOWLEDGEMENT

This work was supported by the Natural Sciences and Engineering Research Council of Canada through Grant No. A1398 received by one of the authors (ACMS), and by the University of New Brunswick.

The authors express their appreciation to Dr. P. M. Gresho and the referees for their comments and suggestions.

NOMENCLATURE

A	area of control volume face
a	discretization coefficient
b	constant part of linearized source term in the finite difference equations
E	time step multiple
P	pressure
p	prolongation operator
P^*	best estimate of pressure
P'	pressure correction
r	restriction operator
Re	Reynolds number based on the top moving wall.
$\|r_P\|$	Euclidean norm of the residual of the pressure correction equation
S	variable dependent part of linearized source term
t	time
$u_i (i = 1, 2)$	velocity components
$u_i^* (i = 1, 2)$	velocity based on P*
$u_i' (i = 1, 2)$	velocity corrections
W	number of work units
$x_i (i = 1, 2)$	Cartesian co-ordinates

Greek letters

α	underrelaxation factor
γ_P	residual reduction factor for the pressure correction equation
Δt	time step
Δt^*	reference time interval
ΔV	volume of the control domain
η	convergence rate
Φ	general dependent variable

Subscripts

E, N, P, S, W	grid points
e, n, s, w	control volume faces
k	grid level
nb	neighbour grid points

Superscripts

N	iteration level

REFERENCES

1. H. Iacovides and B. E. Launder, 'PSL—an economical approach to the numerical analysis of near-wall, elliptic flow', *Trans. ASME, J. Fluids Engng.*, **106,** 241–242 (1984).
2. B. E. Launder, 'Numerical computation of convective heat transfer in complex turbulent flows: time to abandon wall functions?', *Int. J. Heat Mass Transfer*, **27,** (9), 1485–1491 (1984).
3. J. P. Van Doormaal and G. Raithby, 'Enhancements of the SIMPLE method for predicting incompressible fluid flows', *Numer. Heat Transfer*, **7,** 147–163 (1984).
4. A. Brandt, 'Multi-Level adaptive solutions to boundary value problems', *Math. Comput.*, **31,** 333–390 (1977).
5. S. Tuann and M. D. Olson, 'Review of computing methods for recirculating flows', *J. Comput. Phys.*, **29,** 1–19 (1978).
6. V. Ghia, K. N. Ghia and C. T. Shin, 'High-*Re* solutions for incompressible flow using the Navier–Stokes equations and a multigrid method', *J. Comput. Phys.*, **48,** 387–411 (1982).
7. F. H. Harlow and J. E. Welsh, 'Numerical calculation of time-dependent viscous incompressible flow of fluid with free surface', *Phys. Fluids*, **8,** (12), 2182–2189 (1965).
8. D. B. Spalding, 'A novel finite-difference formulation for differential expressions involving both first and second derivatives', *Int. J. numer. methods eng.*, **4**, 551–559 (1972).
9. A. C. M. Sousa and G. V. Hadjisophocleous, 'Numerical studies of convective flows driven by discrete sources', in C. Taylor, M. D. Olson, *Numerical Methods in Laminar and Turbulent Flow, Part 1*,P. M. Gresho and W. G. Habashi (eds), Pineridge Press, Swanseas, U.K., 1985, pp. 901–912.
10. S. V. Patankar, *Numerical Heat Transfer and Fluid Flow*', Hemisphere, New York, N. Y., 1980.
11. G. D. Raithby and G. E. Schneider, 'Numerical solutions of problems in incompressible fluid flow: treatment of the velocity–pressure coupling', *Numer. Heat Transfer*, **2,** (2) 417–440 (1979).
12. G. D. Raithby and K. E. Torrance, 'Upstream-weighted differencing schemes and their application to elliptic problems involving fluid flow', *Computers and Fluids*, **2,** (2), 191–206. (1974).
13. Z. Mazhar and G. D. Raithby, 'A refined PUMPIN method for updating pressure in the numerical solution of the incompressible fluid flow equations', in C. Taylor and B. A. Schrefler (eds), *Numerical Methods for Laminar and Turbulent Flow*, Pineridge Press, Swansea, U.K., 1981, pp. 255–266.
14. A. Brandt, 'Multi-level adaptive computations in fluid dynamics', *AIAA Journal*, **18,** (10), 1165–1172 (1980).
15. W. Hackbusch, 'Introduction of multi-grid methods for the numerical solution of boundary value problems', in J. A. Essevs (ed.), *Computational Methods for Turbulent, Transonic, and Viscous Flows*, Hemisphere, 1983, pp. 45–92.
16. A. C. M. Sousa and D. D. LeBlanc, 'Shell-side flow prediction of an experimental heat exchanger', in C. Taylor, E. Hinton, D. R. J. Owen and E. Onate (eds), Numerical Methods for Nonlinear Problems, Vol. 2, Pineridge Press, Swansea, U.K.. 1984, pp. 791–801.

Requests for reprints should be addressed to Professor A. C. M. Sousa.